Article

Colloids of Naked CH$_3$NH$_3$PbBr$_3$ Perovskite Nanoparticles: Synthesis, Stability, and Thin Solid Film Deposition

Soranyel Gonzalez-Carrero,[†] Luciana C. Schmidt,[†,‡] Ignacio Rosa-Pardo,[†] Laura Martínez-Sarti,[†] Michele Sessolo,[†] Raquel E. Galian,*[,†] and Julia Pérez-Prieto*[,†]

[†]ICMOL, Institute of Molecular Science, Universidad de Valencia, Catedrático José Beltrán 2, 46980 Paterna, Valencia, Spain
[‡]INFIQC (UNC-CONICET), Dpto. Química Orgánica, Facultad de Ciencias Químicas, Universidad Nacional de Córdoba, Ciudad Universitaria, X5000HUA Córdoba, Argentina

S *Supporting Information*

ABSTRACT: A novel preparation of lead halide, CH$_3$NH$_3$PbBr$_3$, perovskite nanoparticle solid films from colloidal "naked" nanoparticles, that is, dispersible nanoparticles without any surfactant, is reported. The colloids are obtained by simply adding potassium ions, whose counterions are both more lipophilic and less coordinating than bromide ions, to the perovskite precursor solutions (CH$_3$NH$_3$Br/ PbBr$_2$ in dimethylformamide) following the reprecipitation strategy. The naked nanoparticles exhibit a low tendency to aggregate in solution, and they effectively self-assembled on a substrate by centrifugation of the colloid, leading to homogeneous nanoparticle solid films with arbitrary thickness. These results are expected to spur further the interest in lead halide perovskites due to the new opportunities offered by these films.
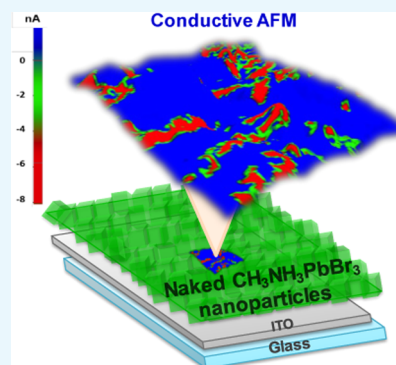
INTRODUCTION

Lead halide perovskites, with the general chemical formula APbX$_3$, where A is an organic or inorganic monovalent cation—in particular methylammonium (CH$_3$NH$_3^+$, MA), formamidinium (HC(NH$_2$)$_2^+$), and Cs$^+$—and X is the halide anion (Cl$^-$, Br$^-$, or I$^-$), have been extensively studied mainly due to their exceptional optoelectronic properties.[1−5] These are attractive materials because of their ease of processability for mass production, such as the preparation of conductive films from solutions of perovskite precursors. This strategy can produce some weaknesses in the end product (polycrystallinity, structural, and chemical defects) and often suffers from a lack of reproducibility of the film morphology.

Therefore, there is a great interest in the direct film preparation from colloidal perovskite nanoparticles (NPs), aimed at high reproducibility of the film morphology as well as improvement of their optoelectronic properties. There are important challenges to be overcome for achieving those goals in the case of lead halide perovskites: the preparation of organic ligand-free perovskite NPs with a low tendency to aggregate in solution and the efficient self-assembling of the perovskite NPs on a substrate to lead to conductive NP solid films with controlled thicknesses.

CH$_3$NH$_3$PbBr$_3$ colloids were first reported in 2014, by using medium and long alkylammonium bromide as the organic capping to confine the material to the nanometer scale and enable their dispersibility in low-to-medium polar organic solvents.[6] Since then, the variations in their preparation, use of other ammonium bromides, ammonium carboxylates, instead

of ammonium bromides, and different molar ratios between the reagents have provided high control on their crystallization, composition, shape, size, and, consequently, on their optical performance.[7−15]

The passivation of the perovskite nanoparticles with organic ligands hampers the preparation of conductive thin films, and consequently there is an increasing interest in developing strategies for synthesizing stable "naked" colloidal nanoparticles. The synthesis of organic ligand-free CH$_3$NH$_3$PbX$_3$ colloids is challenging. An interesting two-step approach has recently been reported to prepare CH$_3$NH$_3$PbX$_3$ (X = Br, I, and mixture of them) colloids of 100 nm to 1 μm, depending on the nature of X. It consisted of the mixing of PbX$_2$ NPs of tens of nanometers (prepared by laser ablation) with isopropanol solutions of CH$_3$NH$_3$X under vigorous sonication and mild heating.[16] The detection in the PbX$_2$ NPs of excess of halide as well as carbon material, derived from the solvent (iodobenzene or bromobenzene) decomposition under laser ablation, was suggested to be responsible for the confinement of the PbX$_2$ material to the nanometer scale.[17] Whereas the carbon materials did not prevent the formation of the hybrid perovskite after addition of the methylammonium halide, the nanoparticle size drastically increased and perovskite particles of hundreds of nanometers were formed.
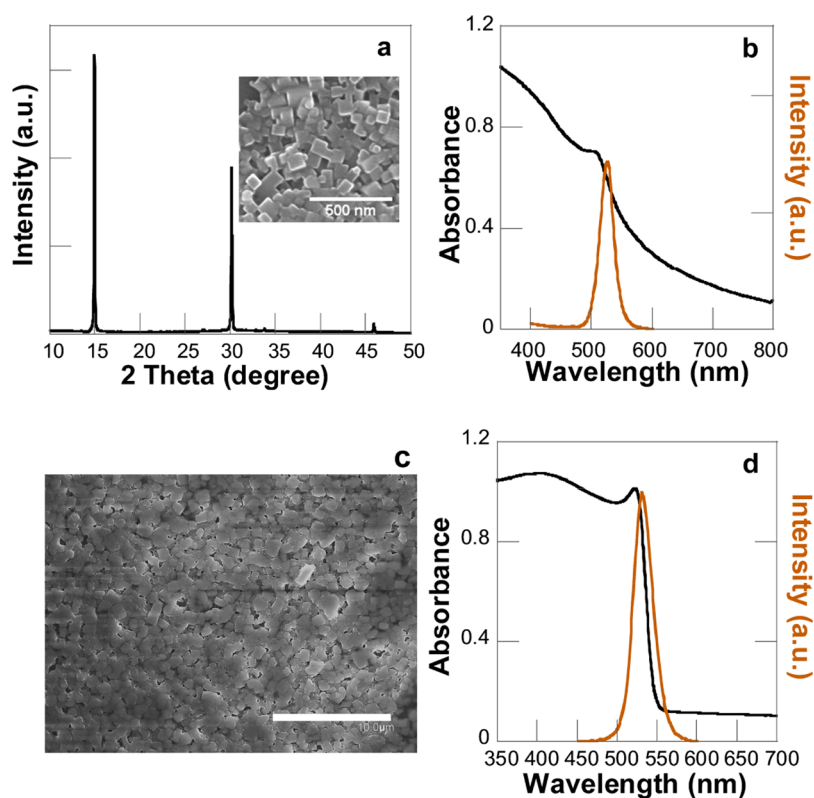
Figure 1. (a) PXRD of MAP@K NPs deposited on quartz revealing its (001) orientation; inset: SEM image of MAP@K NP solid (scale bar: 500 mm). (b) Absorption and emission spectra of MAP@K colloid in ethyl acetate. (c) SEM image of MAP@K$_{F3}$ (scale bar: 10 μm). (d) Absorption and emission spectra of MAP@K$_{F3}$.

Our aim was to use a simple, one-step procedure to prepare naked $CH_3NH_3PbBr_3$ colloidal NPs and assemble them in conductive thin films. We devised that the colloids could be directly prepared by using inorganic salts as the confinement agents. We report here an easy preparation method of naked $CH_3NH_3PbBr_3$ NPs by simply using an excess of CH_3NH_3Br in the perovskite precursor solutions ($CH_3NH_3Br/PbBr_2$ in dimethylformamide (DMF)) and a potassium salt, whose counterion is both more lipophilic and less coordinating than that of the bromide (specifically, hexafluorophosphate anion PF_6^-). The purpose was to replace the excess of $CH_3NH_3^+$ at the $CH_3NH_3PbBr_3$ NP surface with K^+ on the basis of the higher enthalpy formation of KBr than that of CH_3NH_3Br (−394 vs. −259 kJ/mol), with the final aim of producing confined and stable NPs.[18,19] The NPs self-assembled on a substrate under centrifugation of the colloids to lead to homogeneous and conductive NP films.

RESULTS AND DISCUSSION

The colloidal $CH_3NH_3PbBr_3$ methylammonium bromide (MAP) NPs were prepared by using the reprecipitation strategy.[9,11] In brief, a mixture of CH_3NH_3Br, KPF_6, and $PbBr_2$ in DMF (2:2:1 $CH_3NH_3Br/KPF_6/PbBr_2$ molar ratio) was used as the precursor solution. An aliquot of this solution was added dropwise to a moderately polar solvent (ethyl acetate) under vigorous stirring to lead to a yellowish dispersion (see details in the Materials and Methods). After centrifugation, a luminescent yellow solid was separated and was redispersed in ethyl acetate. The colloid was considerably stable and took about 3 h for the complete precipitation of NPs, which were easily redispersed by manual shaking.

To determine the components of the NPs, both the solid and the residual material after solvent evaporation of the supernatant were dissolved in dimethyl sulfoxide (which reverted the perovskite back into its precursors) and they were analyzed by ^{19}F NMR and ^1H NMR (Figures S1 and S2). ^{19}F NMR spectra showed that all of the PF_6^- anions were in the supernatant in the form of two different salts. This was consistent with the presence of KPF_6 and $CH_3NH_3PF_6$ in the supernatant; in fact, the ^1H NMR spectrum of the supernatant showed signals ascribed to the $CH_3NH_3^+$ cation.

The powder X-ray diffraction (PXRD) pattern of MAP, Figure 1a, deposited on quartz by a centrifugal strategy[20] (see details below) confirmed the exclusive formation of cubic $CH_3NH_3PbBr_3$ NPs with lattice diffraction peaks at 14.9, 30.1, and 45.9° (weak), which can be assigned to the (001), (002), and (003) crystallographic peaks; thus, the film displayed (001) exclusive orientation.[21−24] The estimated crystallite size, calculated by Debye−Scherrer equation, was 69 ± 2 nm. The morphology of MAP was studied by scanning electron microscopy (SEM); the images showed the formation of cubic NPs (inset Figure 1a). The energy dispersive X-ray spectrum (Figure S3) of the MAP deposited on glass demonstrated the presence of K in the perovskite material, and a K/Pb/Br molar ratio of 0.5:1:3.4 was calculated. Therefore, the perovskite is capped with KBr.

The absorption and emission spectra of the colloidal MAP NPs in ethyl acetate (Figure 1b) exhibited features of confined material. Thus, the absorption and emission peaks were at about 505 and 525 nm (full-width at half maximum, fwhm = 28 nm), respectively, considerably blue shifted compared to those of bulk $CH_3NH_3PbBr_3$ (absorption peak at about 540 nm).
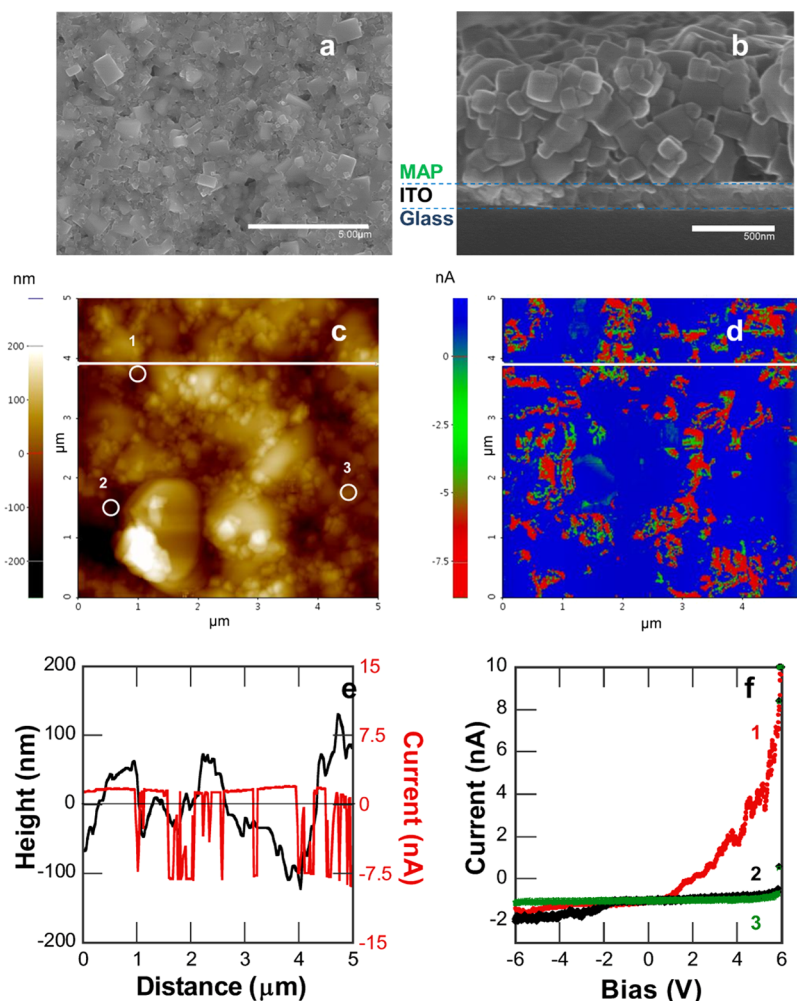
Figure 2. (a) Top and (b) cross-sectional SEM image of MAP@K$_{F4}$ (scale bar 5 μm and 500 nm, respectively). (c, d) Topographical and conductive AFM images of MAP@K$_{F4}$ (bias = −1.5 V); image scale 5 μm × 5 μm. (e) Cross-sectional profile of height and current along the white line in images (c) and (d). (f) I−V curve as a function of applied bias (+6 to −6 V) under dark conditions for grains market in the topographic AFM image c.

The UV−visible maximum at 505 nm was attributed to the exciton peak of the colloidal nanoparticles, whereas the absorption observed above 550 nm could correspond to the scattering of different-sized colloidal aggregates present in solution and absent in the solid film.[11,25] These data corroborated that K$^+$ was on the nanoparticle surface; otherwise, the partial substitution of CH$_3$NH$_3^+$ for K$^+$ in the crystal structure would provoke a shift in the absorption peak to the UV, among other changes.[26] Consequently, these perovskite NPs were termed MAP@K NPs and used for solid film preparation.

The formation of luminescent MAP@K colloids was also observed when using toluene and chlorobenzene in their preparation instead of ethyl acetate (emission peaks at ca. 527 and 525 nm for toluene and chlorobenzene, respectively, Figure S4). However, the NPs remained dispersible for a shorter time (less than 1 h). Therefore, only the stable colloid in ethyl acetate was fully characterized. Photoluminescence (PL) of the MAP@K colloid in ethyl acetate exhibited a quantum yield (Φ_{PL}) of 17% and an average lifetime (τ_{av}) of 29 ns, with a short-lived component of τ_1 3.4 ns (79%) and a long-lived component of τ_2 38 ns (21%).

Control studies were performed to gain further insight into the role of K$^+$ in the stability of the MAP@K NPs. The synthesis of MAP colloids was carried out in the absence of KPF$_6$ under the same experimental conditions. An orange colloidal dispersion, probably assisted by the excess of MA (MA/PbBr$_2$, 2:1), was obtained, but it exhibited a high tendency to precipitate. After centrifugation, the orange pellet could hardly be redispersed in ethyl acetate. In fact, the colloid was stable for just 5 min, and the pellet precipitate was observed at the bottom of the tube (Figure S5). The absorption spectra of the MAP dispersion showed a poor absorption band and high scattering; these features are typical of bulk MAP material prepared using 1:1 MA/PbBr$_2$ molar ratio in the absence of organic ligands.[6] These data demonstrated that K$^+$ participated in the stabilization of the hybrid MAP@K NPs, providing considerably stable colloids in a medium polar solvent and preventing the collapse of NPs.

Attempts to prepare densely packed perovskite nanoparticle solid films from the ethyl acetate MAP@K colloid were addressed by using the centrifugal casting method.[20] Briefly, freshly prepared MAP@K colloids in ethyl acetate were added to a centrifugal tube with a glass substrate at the bottom, and the sample was centrifuged for 7 min. Then, the supernatant

was pipetted out and the MAP@K NP solid film on the glass substrate (MAP@K$_{F1}$; see further details in the Materials and Methods) was allowed to dry at room temperature under ethyl acetate atmosphere. The SEM images showed that the film coverage of the glass substrate was incomplete. Increase of the particle concentration did not result in complete substrate coverage (see MAP@K$_{F2}$ in Figure S6 and details in the Materials and Methods). Interestingly, a complete coverage of the glass substrate was obtained by using a mixture of ethyl acetate and toluene in the centrifugation step; see the SEM image of the film, MAP@K$_{F3}$, in Figure 1c. The film showed an absorption peak at 526 nm and a narrow and slightly red-shifted emission peak at 530 nm (fwhm = 30 nm) compared to that of the MAP@K colloid in ethyl acetate (Figure 1b). The film showed a Φ_{PL} of 7% and a τ_{av} of 97 ns, which fit to three components (τ_1 8.1 ns (60%), τ_2 40.2 ns (31%), and τ_3 170.5 (9%)).[27]

The colloidal dispersion and solid film prepared from MAP@K were stable for at least 1 month when stored in closed-amber vials.

Conductive atomic force microscopy (c-AFM) measurements were carried out in the dark using the PinPoint conductive mode to study the local electronic properties and morphology of an MAP@K NP solid film prepared by centrifugal casting on indium tin oxide (ITO)[20]-coated glass (termed MAP@K$_{F4}$). Figure 2a,b shows the top and cross-sectional SEM images of MAP@K$_{F4}$ and demonstrates the formation of a densely packed nanoparticle solid film of 881 ± 78 nm thickness (see the Materials and Methods and Figure S7 for further details).

The topographical image (area of 25 μm^2) of MAP@K$_{F4}$, Figure 2c, showed protrusions and depressions in the range of +100 to −100 nm (average roughness of 75 nm). The contrast c-AFM image (Figure 2d) revealed a spatial distribution of high and low current magnitude regions, represented in red and blue, respectively. The cross-sectional profile image of height and current along the white line in the topographic and current AFM image (Figure 2e) exhibits high magnitude current domains, between −8.4 and 2.1 nA (average current magnitude −0.447 nA). The c-AFM measurement showed that the vertical current transport was heterogeneous on the nanometer scale, as reported in c-AFM studies of CH$_3$NH$_3$PbX$_3$ films prepared by spin-coating the solution of perovskite precursors.[28−30] Remarkably, the conductivity observed in MAP@K$_{F4}$ was of high magnitude.

The local dark current versus bias (I−V) of MAP@K$_{F4}$ (Figure 2d) was measured at specific locations from the topographic AFM image, identified as round marks in Figure 2c (bias at 6 to −6 V). The local I−V response exhibits a diode behavior, previously observed for millimeter-sized MAPbBr$_3$ crystals.[31,32] Thus, a linear ohmic region at low voltages, where the traps are partially filled; a step-up in current at intermediate voltages, where the traps are filled with injected carriers; and an abrupt increase in current at high voltages, where the carriers move freely, were observed (see curve 1 in Figure 2f). The high conductive domains may be attributed to high-density regions of NPs dispersed in the film with an effective electrical connectivity between them. The charge transport was further investigated at a larger scale by depositing the NP films onto interdigitated indium tin oxide[20] electrodes, with an electrode gap of 20 μm (Figure S8a). The current density versus voltage (J−V) curve in the dark shows current injection in both reverse and forward bias, with current up to 100 nA at voltages as low

as 5 V. The transport properties are comparable to those of a polycrystalline MAPbBr$_3$ film obtained by direct spin-coating of the precursor solution (Figure S8b). Interestingly, when measuring the sample under 1 sun illumination, we observed an increase in the current (up to 5×) and a shift in the J−V curve toward positive bias. The latter effect might originate from a separation of the photogenerated electron−hole pairs. However, considering that the device lacks charge selective contacts and that no photovoltage can be observed under illumination, the shift in the J−V characteristics is probably due to the intrinsic photoconductivity of the perovskite film.

CONCLUSIONS

In summary, we present here an easy preparation method of colloidal stable naked CH$_3$NH$_3$PbBr$_3$ perovskites by adding a potassium salt to the solution of perovskite precursors. The K$^+$ cations on the NP surface stabilize the nanomaterial and the colloid and enable the efficient assembly of nanoparticles on substrates to lead to densely packed, semiconducting nano-particle solid films.

MATERIALS AND METHODS

Materials. Lead bromide (99.999%), methylamine (40% in water), potassium hexafluorophosphate (≥99%), bromidic acid, and the solvents used were purchased from Sigma-Aldrich and used as received. Methylammonium bromide (CH$_3$NH$_3$Br) was synthesized by reaction of the corresponding amine in water/HBr.

Synthesis of Colloidal MAP@K. The precursor solution was prepared by mixing PbBr$_2$ (25 mg, 0.068 mmol), MABr (15.3 mg, 0.14 mmol), and KPF$_6$ (25 mg, 0.14 mmol) in 2.5 mL of dimethylformamide. The molar ratio between the components PbBr$_2$/MABr/KPF$_6$ was 1:2:2. Then, 100 μL was added dropwise into 10 mL of ethyl acetate under vigorous stirring. Immediately after, the yellowish reaction was centrifuged at 7000 rpm for 7 min. The supernatant was discarded, and the precipitate was redispersed in 5 mL of ethyl acetate.

Preparation of MAP@K$_{F1}$ NP Solid Film. Colloidal MAP@K used for the preparation of NP solid films was prepared following the above-mentioned method. The precursor solution was prepared mixing PbBr$_2$ (25 mg, 0.068 mmol), MABr (15.3 mg, 0.14 mmol), and KPF$_6$ (25 mg, 0.14 mmol) in 2.5 mL of dimethylformamide. An aliquot, specifically 100 μL, of this solution was added dropwise into 10 mL of ethyl acetate under vigorous stirring.

Then, the MAP@K colloid (10 mL) was added to a conical centrifuge tube (50 mL), which had the glass slide substrate at its bottom, and the mixture was centrifuged for 7 min at 8000 rpm. Finally, the supernatant was pipetted out and the glass substrate with the deposited MAP@K was allowed to dry in ethyl acetate atmosphere, at room temperature.

Preparation of MAP@K$_{F2}$. The NP solid film was prepared following the method described above for MAP@K$_{F1}$ but using a mixture of two MAP@K colloids (10 mL each).

Preparation of MAP@K$_{F3}$. The NP solid film was prepared following the above-mentioned method for MAP@K$_{F2}$ but adding 10 mL of toluene to 20 mL of MAP@K colloid before the centrifugation step.

Preparation of MAP@K$_{F4}$. The NP solid film was prepared following the above-mentioned method for MAP@K$_{F3}$ but using an ITO-glass-coated substrate.

The glass substrates used were cleaned ultrasonically in water-soap, demineralized water, and 2-propanol baths. Then, they were dried under nitrogen and immediately placed into a conic centrifugal tube. Centrifugation was carried out in an Eppendorf Centrifuge 5804 R.

Preparation of Polycrystalline MAPbBr₃. The precursor solution was prepared mixing $PbBr_2$ and MABr (1:2 ratio, respectively) in dimethylformamide to a total concentration of 100 mg/mL. The solution was spin-coated at 3000 rpm for 60 s. The as-prepared layers were annealed on a hot plate at 90 °C for 30 min in a nitrogen atmosphere glovebox.

Optical Measurement. UV−visible spectra of the samples were recorded using a quartz cuvette in a UV−visible spectrophotometer secoman Uvi Ligth XT5. The UV−vis spectra of NP solid films were recorded in a JASCO V-670 spectrometer with a horizontal integrating sphere (PIV-757). Steady-state PL spectra were measured on an Amnico Browman series 2 Luminescence spectrometer, equipped with a xenon lamp (150 W). AB2 software (version 5.5) was used to register the data. The photoluminescence (PL) quantum yields of colloidal MAP@K (in ethyl acetate) and film were measured using a Hamamatsu C9920-02 absolute PL quantum yield measurement system with monochromatic light source (150 W) and integrating sphere. All of the data were acquired using 1 cm × 1 cm path length quartz cuvettes, at room temperature, using an excitation wavelength of 365 nm.

PL decays were measured using a Compact fluorescence lifetime spectrometer C11367, Quantaurus-Tau. Fluorescence lifetime software U11487 was used to register the data. All of the data of PL decay of perovskite dispersed in ethyl acetate were acquired using 1 cm × 1 cm path length quartz cuvettes and light-emitting diode excitation wavelength of 365 nm. The PL decays of colloidal perovskite nanoparticles were fitted with a triexponential function. The average lifetimes (τ_{av}) were calculated as $\tau_{av} = \sum A_i\tau_i^2/\sum A_i\tau_i$, where τ_i are the decay times and α_i represents the amplitudes of the components, values obtained from the fitted PL kinetic decay traces.

Morphology Characterization. The layer thickness was determined with a mechanical profilometer (Ambios XP-1). Scanning electron microscope[29] images of NP solid films were obtained using a HITACHI S-4800 with a spotlight of field emission gun. Images were acquired at 20 kV. Elemental analysis was performed on HITACHI S-4800 equipped with XFlash 5030 Bruker detector and acquisition software QUANTAX 400. The PXRD analyses of NP solid films were performed in powder diffractometer D8 Advance A25 model Bruker, with a powder diffractometer $\theta-\theta$ configuration, and X-ray tubes on a lineal receiver Cu radiation. Plus DIFFRAC EVA Data assessment program was used to register the data. The diffracted intensities were recorded at room temperature from 5 to 80° 2θ angles (step size of 0.02°).

Conductive Atomic Force Microscopy (c-AFM). The topographic, current mapping, and $I-V$ measurements of NP solid film, MAP@K_{F4}, were registered in dark and at room temperature, in atomic force microscope Park Systems NX20, equipped with Pt−Ir-coated Si tips (CONTSCPt, diameter 7 nm) and using PinPoint conductive mode. The gentle PinPoint mode allowed acquiring reproducible and reliable topography and c-AFM images of the MAP@K_{F4} film surface, instead of contact mode. This PinPoint mode operates in an approach-retract manner. Experimentally, the tip was approached over a period of 2 ms to achieve an interaction force of 0.24 nN; the force was held constant while the current was registered (2

times) at 17 kHz. Then, the tip retracted over a period of 2 ms and moved to the next pixel, Figure S7. The control height (set to 0.15 μm) at constant force was also recorded to generate a simultaneous topographic image. Different voltage biases were applied (from ±1.5 to ±5.5 V) using a scan rate of 0.23 Hz. The PinPoint mode is significantly different from the tapping mode because the contact mode tip used is not oscillating and the tip retracts and approaches each pixel rather than adjusting the tip height to maintain a constant oscillation amplitude, resulting in highly reproducible images. The current is measured directly after the tip using a preamplifier with a gain of 1011 V/A (ULCA). Data acquisition was carried out using SmartScan software (version 1.0) and XEI Data Processing and Analysis software (version 4.3.0) Build2 (Park Systems Corp). The NX20 equipment is supported by active vibration isolation system model AVI-200S/LP (Table Stable Ltd). The $I-V$ images were performed using a current compliance of 10 nA and sample bias from +6 to −6 V with a period of 1.0 s.

Lateral Transport Measurements. The substrates used for these measurements were prepatterned interdigitated ITO electrodes (Naranjosubstrates) coated on glass. The current density−voltage ($J-V$) characteristics were obtained using a Keithley 2400 source measure unit. The electrical characterization was performed in the dark and under illumination using a solar simulator by Abet Technologies (model 10500 with an AM1.5G xenon lamp as the light source). The current density was calculated taking into account the channel width and film thickness.

■ ASSOCIATED CONTENT

ⓢ Supporting Information

The Supporting Information is available free of charge on the ACS Publications website at DOI: 10.1021/acsomega.7b02052.

> Additional information: NMR, absorption and emission spectra, SEM images, energy dispersive X-ray spectroscopy analysis, and $J-V$ curve measurements (PDF)

■ AUTHOR INFORMATION

Corresponding Authors
*E-mail: raquel.galian@uv.es (R.E.G.).
*E-mail: julia.perez@uv.es (J.P.-P.).

ORCID ⊙
Soranyel Gonzalez-Carrero: 0000-0003-2430-4458
Luciana C. Schmidt: 0000-0001-7059-3938
Michele Sessolo: 0000-0002-9189-3005
Raquel E. Galian: 0000-0001-8703-4403
Julia Pérez-Prieto: 0000-0002-5833-341X

Notes

The authors declare no competing financial interest.

■ ACKNOWLEDGMENTS

■ REFERENCES

(1) Kojima, A.; Teshima, K.; Shirai, Y.; Miyasaka, T. Organometal Halide Perovskites as Visible-Light Sensitizers for Photovoltaic Cells. *J. Am. Chem. Soc.* **2009**, *131*, 6050−6051.

(2) Lee, M. M.; Teuscher, J.; Miyasaka, T.; Murakami, T. N.; Snaith, H. J. Efficient Hybrid Solar Cells Based on Meso-Superstructured Organometal Halide Perovskites. *Science* **2012**, *338*, 643−647.

(3) González-Carrero, S.; Galian, R. E.; Pérez-Prieto, J. Organometal Halide Perovskites: Bulk Low-Dimension Materials and Nanoparticles. *Part. Part. Syst. Charact.* **2015**, *32*, 709−720.

(4) Manser, J. S.; Christians, J. A.; Kamat, P. V. Intriguing Optoelectronic Properties of Metal Halide Perovskites. *Chem. Rev.* **2016**, *116*, 12956−13008.

(5) Fu, A.; Yang, P. Organic-inorganic perovskites: Lower threshold for nanowire lasers. *Nat. Mater.* **2015**, *14*, 557−558.

(6) Schmidt, L. C.; Pertegás, A.; González-Carrero, S.; Malinkiewicz, O.; Agouram, S.; Mínguez Espallargas, G.; Bolink, H. J.; Galian, R. E.; Pérez-Prieto, J. Nontemplate Synthesis of $CH_3NH_3PbBr_3$ Perovskite Nanoparticles. *J. Am. Chem. Soc.* **2014**, *136*, 850−853.

(7) Gonzalez-Carrero, S.; Galian, R. E.; Perez-Prieto, J. Maximizing the emissive properties of $CH_3NH_3PbBr_3$ perovskite nanoparticles. *J. Mater. Chem. A* **2015**, *3*, 9187−9193.

(8) Zhang, F.; Zhong, H.; Chen, C.; Wu, X.-g.; Hu, X.; Huang, H.; Han, J.; Zou, B.; Dong, Y. Brightly Luminescent and Color-Tunable Colloidal CH3NH3PbX3 (X = Br, I, Cl) Quantum Dots: Potential Alternatives for Display Technology. *ACS Nano* **2015**, *9*, 4533−4542.

(9) Huang, H.; Susha, A. S.; Kershaw, S. V.; Hung, T. F.; Rogach, A. L. Control of Emission Color of High Quantum Yield $CH_3NH_3PbBr_3$ Perovskite Quantum Dots by Precipitation Temperature. *Adv. Sci.* **2015**, *2*, No. 1500194.

(10) Huang, H.; Polavarapu, L.; Sichert, J. A.; Susha, A. S.; Urban, A. S.; Rogach, A. L. Colloidal lead halide perovskite nanocrystals: synthesis, optical properties and applications. *NPG Asia Mater.* **2016**, *8*, No. e328.

(11) Gonzalez-Carrero, S.; Francés-Soriano, L.; González-Béjar, M.; Agouram, S.; Galian, R. E.; Pérez-Prieto, J. The Luminescence of CH3NH3PbBr3 Perovskite Nanoparticles Crests the Summit and Their Photostability under Wet Conditions is Enhanced. *Small* **2016**, *12*, 5245−5250.

(12) Vybornyi, O.; Yakunin, S.; Kovalenko, M. V. Polar-solvent-free colloidal synthesis of highly luminescent alkylammonium lead halide perovskite nanocrystals. *Nanoscale* **2016**, *8*, 6278−6283.

(13) Levchuk, I.; Osvet, A.; Tang, X.; Brandl, M.; Perea, J. D.; Hoegl, F.; Matt, G. J.; Hock, R.; Batentschuk, M.; Brabec, C. J. Correction to Brightly Luminescent and Color-Tunable Formamidinium Lead Halide Perovskite FAPbX3 (X = Cl, Br, I) Colloidal Nanocrystals. *Nano Lett.* **2017**, *17*, 3993.

(14) Lu, C.-H.; Hu, J.; Shih, W. Y.; Shih, W.-H. Control of morphology, photoluminescence, and stability of colloidal methyl-ammonium lead bromide nanocrystals by oleylamine capping molecules. *J. Colloid Interface Sci.* **2016**, *484*, 17−23.

(15) Teunis, M. B.; Johnson, M. A.; Muhoberac, B. B.; Seifert, S.; Sardar, R. Programmable Colloidal Approach to Hierarchical Structures of Methylammonium Lead Bromide Perovskite Nanocryst-als with Bright Photoluminescent Properties. *Chem. Mater.* **2017**, *29*, 3526−3537.

(16) Lamberti, F.; Litti, L.; De Bastiani, M.; Sorrentino, R.; Gandini, M.; Meneghetti, M.; Petrozza, A. High-Quality, Ligands-Free, Mixed-Halide Perovskite Nanocrystals Inks for Optoelectronic Applications. *Adv. Energy Mater.* **2017**, *7*, No. 1601703.

(17) Amendola, V.; Polizzi, S.; Meneghetti, M. Laser Ablation Synthesis of Gold Nanoparticles in Organic Solvents. *J. Phys. Chem. B* **2006**, *110*, 7232−7237.

(18) Pedley, J. B. *Thermochemical Data and Structures of Organic Compounds*. Thermodynamics Research Center: College Station, TX, 1994.

(19) Lide, D. R. *CRC Handbook of Chemistry and Physics*, 85th ed.; Taylor & Francis, 2004.

(20) Kim, J. Y.; Adinolfi, V.; Sutherland, B. R.; Voznyy, O.; Kwon, S. J.; Kim, T. W.; Kim, J.; Ihee, H.; Kemp, K.; Adachi, M.; Yuan, M.; Kramer, I.; Zhitomirsky, D.; Hoogland, S.; Sargent, E. H. Single-step fabrication of quantum funnels via centrifugal colloidal casting of nanoparticle films. *Nat. Commun.* **2015**, *6*, No. 7772.

(21) Chen, F.; Zhu, C.; Xu, C.; Fan, P.; Qin, F.; Gowri Manohari, A.; Lu, J.; Shi, Z.; Xu, Q.; Pan, A. Crystal structure and electron transition underlying photoluminescence of methylammonium lead bromide perovskites. *J. Mater. Chem. C* **2017**, *5*, 7739−7745.

(22) Baikie, T.; Barrow, N. S.; Fang, Y.; Keenan, P. J.; Slater, P. R.; Piltz, R. O.; Gutmann, M.; Mhaisalkar, S. G.; White, T. J. A combined single crystal neutron/X-ray diffraction and solid-state nuclear magnetic resonance study of the hybrid perovskites $CH_3NH_3PbX_3$ (X = I, Br and Cl). *J. Mater. Chem. A* **2015**, *3*, 9298−9307.

(23) Peng, W.; Wang, L.; Murali, B.; Ho, K.-T.; Bera, A.; Cho, N.; Kang, C.-F.; Burlakov, V. M.; Pan, J.; Sinatra, L.; Ma, C.; Xu, W.; Shi, D.; Alarousu, E.; Goriely, A.; He, J.-H.; Mohammed, O. F.; Wu, T.; Bakr, O. M. Solution-Grown Monocrystalline Hybrid Perovskite Films for Hole-Transporter-Free Solar Cells. *Adv. Mater.* **2016**, *28*, 3383−3390.

(24) Zhang, Z.-Y.; Wang, H.-Y.; Zhang, Y.-X.; Li, K.-J.; Zhan, X.-P.; Gao, B.-R.; Chen, Q.-D.; Sun, H.-B. Size-dependent one-photon- and two-photon-pumped amplified spontaneous emission from organo-metal halide CH3NH3PbBr3 perovskite cubic microcrystals. *Phys. Chem. Chem. Phys.* **2017**, *19*, 2217−2224.

(25) Chirvony, V. S.; González-Carrero, S.; Suárez, I.; Galian, R. E.; Sessolo, M.; Bolink, H. J.; Martínez-Pastor, J. P.; Pérez-Prieto, J. Delayed Luminescence in Lead Halide Perovskite Nanocrystals. *J. Phys. Chem. C* **2017**, *121*, 13381−13390.

(26) Tarasova, A. Y.; Isaenko, L. I.; Kesler, V. G.; Pashkov, V. M.; Yelisseyev, A. P.; Denysyuk, N. M.; Khyzhun, O. Y. Electronic structure and fundamental absorption edges of KPb2Br5, K0.5Rb0.5Pb2Br5, and RbPb2Br5 single crystals. *J. Phys. Chem. Solids* **2012**, *73*, 674−682.

(27) Zhang, X.; Liu, H.; Wang, W.; Zhang, J.; Xu, B.; Karen, K. L.; Zheng, Y.; Liu, S.; Chen, S.; Wang, K.; Sun, X. W. Hybrid Perovskite Light-Emitting Diodes Based on Perovskite Nanocrystals with Organic-Inorganic Mixed Cations. *Adv. Mater.* **2017**, *29*, No. 1606405.

(28) Moerman, D.; Eperon, G. E.; Precht, J. T.; Ginger, D. S. Correlating Photoluminescence Heterogeneity with Local Electronic Properties in Methylammonium Lead Tribromide Perovskite Thin Films. *Chem. Mater.* **2017**, *29*, 5484−5492.

(29) Kutes, Y.; Zhou, Y.; Bosse, J. L.; Steffes, J.; Padture, N. P.; Huey, B. D. Mapping the Photoresponse of $CH_3NH_3PbI_3$ Hybrid Perovskite Thin Films at the Nanoscale. *Nano Lett.* **2016**, *16*, 3434−3441.

(30) Lee, B.; Lee, S.; Cho, D.; Kim, J.; Hwang, T.; Kim, K. H.; Hong, S.; Moon, T.; Park, B. Evaluating the Optoelectronic Quality of Hybrid Perovskites by Conductive Atomic Force Microscopy with Noise Spectroscopy. *ACS Appl. Mater. Interfaces* **2016**, *8*, 30985−30991.

(31) Shi, D.; Adinolfi, V.; Comin, R.; Yuan, M.; Alarousu, E.; Buin, A.; Chen, Y.; Hoogland, S.; Rothenberger, A.; Katsiev, K.; Losovyj, Y.; Zhang, X.; Dowben, P. A.; Mohammed, O. F.; Sargent, E. H.; Bakr, O. M. Low trap-state density and long carrier diffusion in organolead trihalide perovskite single crystals. *Science* **2015**, *347*, 519.

(32) Yang, K.; Li, F.; Veeramalai, C. P.; Guo, T. A facile synthesis of $CH_3NH_3PbBr_3$ perovskite quantum dots and their application in flexible nonvolatile memory. *Appl. Phys. Lett.* **2017**, *110*, No. 083102.